

1      **Awake ripples enhance emotional memory encoding in the human brain**

2

3      Haoxin Zhang<sup>1,2\*#</sup>, Ivan Skelin<sup>1#</sup>, Shiting Ma<sup>1</sup>, Michelle Paff<sup>3</sup>, Michael A.

4      Yassa<sup>1,4,5</sup>, Robert T. Knight<sup>6,7</sup> & Jack J. Lin<sup>1,2,8\*</sup>

5

6      <sup>1</sup>*Department of Neurology, University of California Irvine, Irvine, 92603, CA, USA*

7      <sup>2</sup>*Department of Biomedical Engineering, University of California Irvine, Irvine, 92603,*  
8      *CA, USA*

9      <sup>3</sup>*Department of Neurosurgery, University of California Irvine, Irvine, 92603, CA, USA*

10     <sup>4</sup>*Department of Neurobiology and Behavior, University of California Irvine, Irvine,*  
11     *92603, CA, USA*

12     <sup>5</sup>*Department of Psychological Science, University of California Irvine, Irvine, 92603,*  
13     *CA, USA*

14     <sup>6</sup>*Department of Psychology, University of California Berkeley, 130 Barker Hall,*  
15     *Berkeley, 94720, CA, USA*

16     <sup>7</sup>*Helen Wills Neuroscience Institute, University of California Berkeley, Berkeley, 94720,*  
17     *CA, USA*

18     <sup>8</sup>*Department of Anatomy and Neurobiology, University of California Irvine, Irvine, 92603,*  
19     *CA, USA*

---

20

21     \* Corresponding author

22     E-mail: [haoxinz1@uci.edu](mailto:haoxinz1@uci.edu)

23     E-mail: [linjj@hs.uci.edu](mailto:linjj@hs.uci.edu)

24     # Equal contribution

25

26 **Abstract**

27

28        Intracranial recordings from the human amygdala and the hippocampus during an  
29 emotional memory encoding and discrimination task reveal increased awake sharp-  
30 wave/ripples (aSWR) after encoding of emotional compared to neutral stimuli. Further,  
31 post-encoding aSWR-locked memory reinstatement in the amygdala and the  
32 hippocampus was predictive of later memory discrimination. These findings provide  
33 electrophysiological evidence that post-encoding aSWRs enhance memory for emotional  
34 events.

35 **Main**

36

37       Multiple mechanisms have been proposed to explain the prioritized encoding of  
38 emotional experiences<sup>1-3</sup>, including the neuromodulatory effects on plasticity and the  
39 interplay between the amygdala and the hippocampus<sup>1,4,5</sup>. Several studies have found  
40 memory reinstatement during the immediate post-encoding period to be predictive of later  
41 memory performance<sup>6,7</sup>. Sharp-wave/ripples (SWRs) are transient hippocampal  
42 oscillations (80-150 Hz), associated with synchronous neural activation in the  
43 hippocampus and the amygdala<sup>8,9</sup>, and are implicated in the binding of anatomically  
44 distributed memory traces<sup>10</sup>. Behaviorally relevant reactivation of emotional memory  
45 occurs during aSWRs<sup>11</sup>, and disruptions of post-experience aSWR interfere with memory  
46 utilization<sup>12</sup>. Based on these findings, we hypothesized that aSWRs occurring  
47 immediately after stimulus encoding (post-encoding) facilitate emotional memory  
48 discrimination through the coordinated hippocampal-amygdala memory reinstatement.  
49 Using intracranial electroencephalographic (iEEG) recordings in epilepsy patients during  
50 the performance of an emotional encoding and discrimination task, we first confirm  
51 reports of better discrimination memory for arousing stimuli<sup>3</sup>. Next, we demonstrate that  
52 the number of aSWR events immediately after encoding is associated with both stimulus-  
53 induced arousal and the accuracy of later discrimination. Finally, the coordinated memory  
54 reinstatement between the amygdala and the hippocampus during post-encoding aSWRs  
55 is predictive of later memory discrimination performance, with the amygdala  
56 reinstatement showing a directional influence on the hippocampal reinstatement.  
57 Together, these findings provide evidence for aSWRs-mediated memory reinstatement in  
58 the amygdala and hippocampus as a mechanism accounting for better remembering of  
59 emotional experiences.

60

61       We performed simultaneous iEEG recordings from the amygdala ( $n_{electrode} = 20$ ) and  
62 the hippocampus ( $n_{electrode} = 17$ , Fig. 2a) in 7 human subjects, while performing an  
63 emotional memory encoding and discrimination task<sup>13,14</sup> (Methods, Fig. 1a). During the  
64 encoding stage, subjects were presented with a stimulus (image; stimulus encoding) and  
65 asked to rate the stimulus valence as negative, neutral, or positive (post-  
66 encoding/response). During the retrieval stage, subjects were presented with one of the 3  
67 types of stimuli - Repeats (identical), Lure (slightly different) or Novel (stimuli not seen  
68 during encoding) - and classified each stimulus as "New" or "Old."

69

70       Memory discrimination is defined as the correct classification of: 1) Repeat stimuli as  
71       Old, 2) Novel stimuli as New, or 3) Lure stimuli as New. Subjects classified Repeat stimuli  
72       and Novel stimuli with high accuracy (Repeat:  $89.4 \pm 2.4\%$ , Novel:  $93.9 \pm 1.4\%$ ; Fig. 1b).  
73       Memory discrimination accuracy was lower for Lure stimuli, relative to both Repeat or  
74       Novel stimuli (Lure:  $61.5 \pm 3.7\%$ ;  $p_{\text{Novel vs Lure}} < 0.001$ ,  $t = 8.36$ ;  $p_{\text{Repeat vs Lure}} < 0.001$ ,  $t =$   
75       6.13, paired t-test), reflecting similarity-induced memory interference. Indeed, there was a  
76       strong negative association between subjects' stimulus discrimination ability and stimulus  
77       similarity rating ( $p = 0.039$ ,  $t = -2.06$ , see Methods, Fig. 1c-d). Stimulus-induced arousal  
78       (irrespective of valence) was associated with better memory discrimination, confirming  
79       previous reports<sup>1-3</sup> ( $p = 0.047$ ,  $t = 1.98$ , Fig. 1c-d, Extended Data Fig. 1).

80

81       We defined the post-encoding period as the interval between stimulus offset and  
82       subjects' stimulus valence rating response (Fig. 1a). We tested the association of post-  
83       encoding aSWR occurrence (i.e., the number of aSWRs) with the stimulus emotional  
84       content (stimulus-induced arousal and valence) and correct discrimination during  
85       retrieval. Higher post-encoding aSWR occurrence was associated with stimulus-induced  
86       arousal ( $p = 0.03$ ,  $z = -2.2$ , Wilcoxon signed-rank test, Fig. 2c) and also predicted correct  
87       discrimination during retrieval ( $p = 0.03$ ,  $z = -2.2$ , Wilcoxon signed-rank test, Fig. 2c), but  
88       was not associated with stimulus valence ( $p = 0.77$ ,  $F(2, 15) = 0.25$ , one-way ANOVA;  
89       Extended Data Fig. 3). Taken together, these results provide the first report of post-  
90       encoding aSWRs as a potential electrophysiological mechanism for enhanced memory  
91       discrimination of arousing stimuli, previously characterized at behavioral level<sup>2,3,15</sup>.  
92       Furthermore, the positive associations between aSWRs and stimulus-induced  
93       arousal/later discrimination were present in all individual subjects (Fig. 2c). The post-  
94       encoding response time (RT) did not differ based on stimulus-induced arousal ( $p = 0.2$ ,  $z$   
95       = 0.7,  $RT_{\text{high-arousal}} = 0.8 \pm 0.1$  sec;  $RT_{\text{low-arousal}} = 0.6 \pm 0.2$  sec) or later discrimination ( $p =$   
96       0.25,  $z = 0.6$ ,  $RT_{\text{correct}} = 0.7 \pm 0.2$  sec,  $RT_{\text{incorrect}} = 0.7 \pm 0.3$ , Wilcoxon signed-rank test).  
97       Therefore, the associations between stimulus-induced arousal or correct discrimination  
98       and post-encoding aSWR occurrence were unrelated to post-encoding duration.  
99       Associations between aSWR and stimulus-induced arousal/later correct discrimination  
100      accuracy were selective for the post-encoding time window. These relationships were  
101      absent for the stimulus encoding or the retrieval task stage ( $p > 0.05$ , Wilcoxon signed-  
102      rank test; Fig. 2c, Extended Data Fig. 3, 4). The aSWRs probability was significantly

103 higher during low theta power periods (Extended Data Fig. 5), consistent with  
104 observations that cholinergic tone promotes theta oscillations and suppresses SWRs<sup>10,12</sup>.  
105 In addition, aSWRs did not overlap with increased broadband gamma power, suggesting  
106 that aSWRs are distinct from non-specific broadband power fluctuations<sup>16</sup> (Extended Data  
107 Fig. 5).

108

109       Recent studies suggest that post-encoding memory reinstatement supports  
110 successful subsequent memory retrieval<sup>6,7</sup>. Meanwhile SWR is associated with  
111 reactivation of pre-established neuronal patterns<sup>17</sup>. We hypothesized that memory  
112 reinstatement during the post-encoding aSWR window could enhance later memory  
113 discrimination. Distinct neural populations have been proposed to represent individual  
114 stimuli, resulting in stimulus-specific high-frequency activity (HFA) patterns<sup>18,19</sup>. We, thus,  
115 quantified memory reinstatement as the Spearman correlation between HFA power  
116 spectral vectors (PSVs), for each combination of the encoding-response time bins from  
117 the same trial (Extended Data Fig. 6). Next, we computed the average reinstatement  
118 activity during  $\pm 250$  msec around post-encoding aSWR peaks. The reinstatement  
119 significance was determined relative to a null distribution, obtained by circular jittering of  
120 aSWR timestamps. The post-encoding aSWR-locked memory reinstatement was  
121 stronger for arousing and correctly discriminated stimuli (Extended Data Fig. 7). To  
122 assess specific contributions of the amygdala and the hippocampus to this phenomenon,  
123 we calculated post-encoding memory reinstatement for each region, relative to aSWR  
124 peak (Fig. 3a). The significant reinstatement period in the amygdala consisted of two  
125 intervals, the first starting slightly earlier and overlapping with the hippocampal  
126 reinstatement (-105 to -50 msec), and a second period following the hippocampal  
127 reinstatement (40 to 200 msec). The significant reinstatement period in the hippocampus  
128 lasted from -100 to 50 msec (Fig. 3b). These results demonstrated region-specific timing  
129 of the post-encoding aSWR-locked memory reinstatement in the amygdala and the  
130 hippocampus. Next, we tested for the temporal compression<sup>17</sup> of post-encoding aSWR-  
131 locked reinstatement (no compression, 2x, 4x, and 6x compression) and showed the  
132 strongest aSWR-locked reinstatement with no compression (Extended Data Fig. 8). We  
133 then analyzed the association of the post-encoding memory reinstatement with the  
134 stimulus-induced arousal and later discrimination. Remarkably, we observed a region-  
135 specific double dissociation. Specifically, the amygdala, not the hippocampus, showed a  
136 positive association between aSWR-locked memory reinstatements and the stimulus-

137 induced arousal (AMY: -80 to -10 msec,  $p = 0.035$ ; HPC:  $p > 0.05$ , see Methods; Fig. 3c).  
138 In contrast, the hippocampus, but not the amygdala, revealed a positive association  
139 between aSWR-locked memory reinstatement and later correct discrimination (AMY:  $p >$   
140 0.05; HPC: -15 to 90 msec,  $p = 0.008$ , see Methods; Fig. 3c). To summarize, post-  
141 encoding aSWR-locked memory reinstatements in the amygdala and the hippocampus  
142 followed distinct temporal dynamics and were associated with reactivation of distinct  
143 aspects of encoded stimuli (i.e., the amygdala for stimulus-induced arousal and the  
144 hippocampus for later discrimination accuracy).

145

146 In rodents, the coordinated memory reactivation in the amygdala and hippocampus  
147 during sleep SWRs is proposed to bind neuronal ensembles encoding emotional and  
148 spatial information, respectively<sup>20</sup>. We reasoned that a similar interaction between the  
149 amygdala and the hippocampus exists in which cross-regional post-encoding aSWR-  
150 locked memory reinstatement facilitates later discrimination. We hypothesized that the  
151 reinstatement in both structures co-occurs during the same aSWR events and follows a  
152 consistent temporal dynamic. To test this, we separately computed aSWR-locked joint  
153 memory reinstatement for the correctly and incorrectly discriminated stimuli (Methods). A  
154 significant joint aSWR-locked memory reinstatement in the amygdala and hippocampus  
155 was present during the post-encoding period only for correctly discriminated stimuli (Fig.  
156 3d; Extended Data Fig. 9). Specifically, the amygdala reinstatement preceded the  
157 hippocampal reinstatement by ~100 msec. Further, mutual information analysis showed a  
158 significant unidirectional influence from the amygdala to the hippocampus before aSWR  
159 peak (-70 to -30 msec,  $p = 0.038$ ; see Methods; Fig. 3e). To conclude, aSWR-mediated  
160 coordination of memory reinstatement in the amygdala and the hippocampus promotes  
161 later successful discrimination.

162

163 Rodent studies have implicated the SWRs in the retrieval and consolidation of  
164 emotional memory. However, it is unclear whether it supports the memory benefits of  
165 emotional experience<sup>21</sup>. Our study reveals an association of higher aSWR occurrence  
166 with stimulus-induced arousal and subsequent correct stimulus discrimination, providing  
167 direct evidence for aSWR-mediated strengthening of emotional memory. Interestingly, the  
168 higher aSWRs occurrence has been shown in rodents, after exposure to a novel or  
169 reward-associated context<sup>22</sup>. Together, this suggests that aSWRs may play a general role  
170 in the selective enhancement of salient experiences<sup>23</sup>.

171

172 Notably, such association is specific to the post-encoding period that starts  
173 immediately after memory encoding, when memory retrieval is essential to rate the  
174 emotional content of the stimuli. This finding supports theoretical assumptions that SWRs  
175 mediate both the retrieval of stored representation utilized in decision-making, and the  
176 strengthening of the same representation, contributing to memory consolidation<sup>22</sup>.

177

178 Next, we aimed to discern the link between the aSWR-associated interaction between  
179 the amygdala and hippocampus during post-encoding and subsequent memory effect.  
180 We found the aSWRs were accompanied by memory reinstatement during the post-  
181 encoding period. Specifically, the reinstatement in the amygdala appears shortly before  
182 the aSWR peak and shows association with arousing stimuli, while the hippocampal  
183 reinstatement appears around the aSWR peak and shows associations with correct  
184 subsequent memory discrimination. Moreover, the co-occurrence of the amygdala and  
185 the hippocampal reinstatement during the same post-encoding aSWR events - with the  
186 amygdala reinstatement leading hippocampal by ~100 msec - is predictive of subsequent  
187 correct memory discrimination. This finding suggests that the coordinated reinstatement  
188 in the amygdala and hippocampus during aSWR is responsible for combining emotional  
189 and contextual aspects of the memory<sup>20,21</sup>.

190

191 Both the joint-reinstatement and mutual information analyses further confirm the  
192 predictive validity of directional influence from the amygdala to the hippocampus before  
193 aSWRs on correct discrimination, establishing a link between the amygdala reinstatement  
194 and memory discrimination as a physiological mechanism of emotional memory  
195 enhancement. Together, our data support a model wherein the memory reinstatement in  
196 the amygdala, triggered by emotional stimuli, elicits amygdala-hippocampal aSWR-  
197 associated memory reinstatement, enabling the coordinated joint-reinstatement, which  
198 facilitates subsequent memory performance.

199

## 200 Acknowledgement

201 The authors thank all the participants for taking part in the study, as well as the  
202 nurses, technicians, and physicians at the UCI Epilepsy Unit. This work was supported by  
203 NIH Grant 1U19NS107609-01 to R.T.K. (subcontract to J.J.L).

204

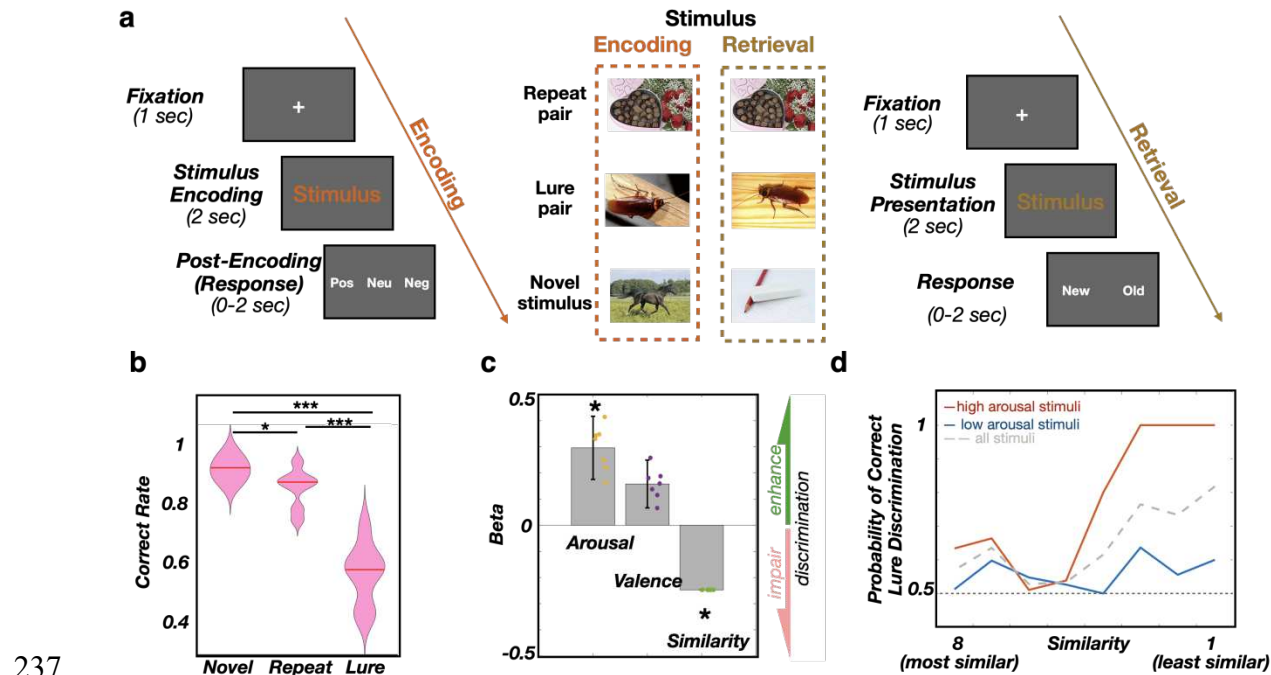
205 **Competing Interests statement**

206 The authors declare no competing interest.

207

208 **References**

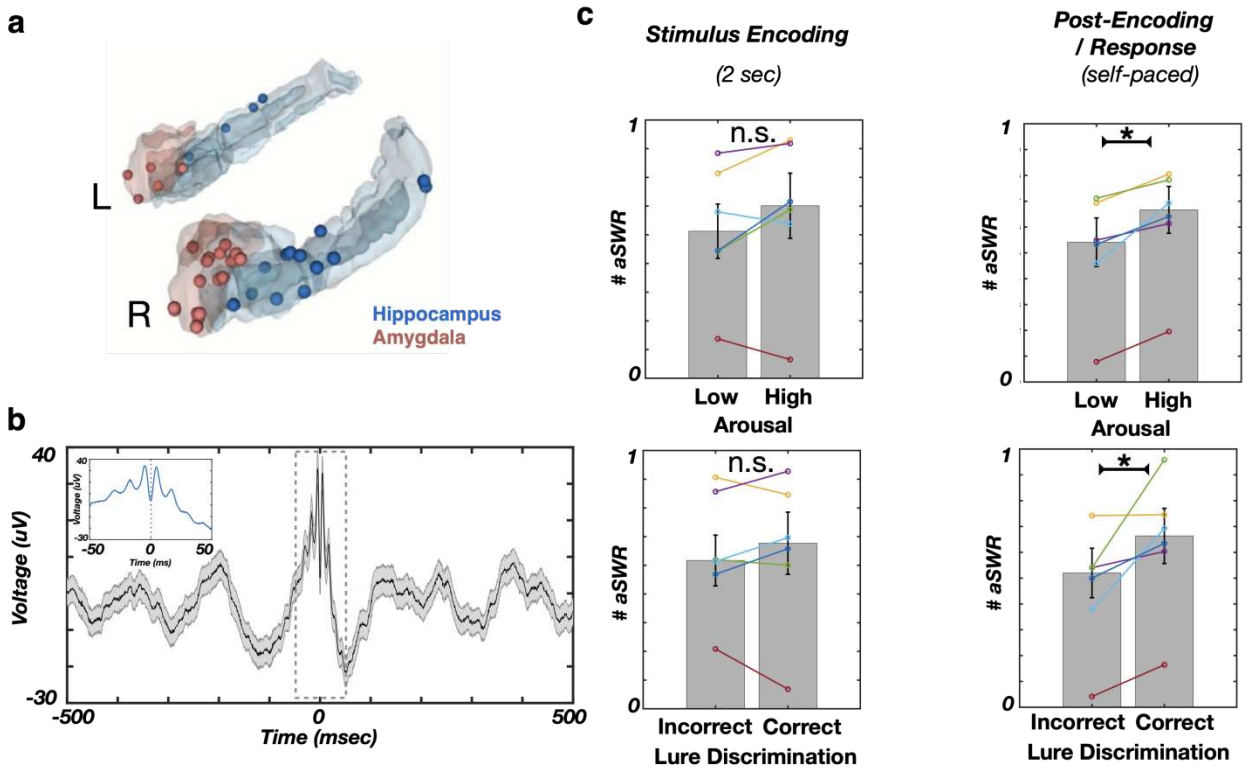
- 209 1. Cahill, L., Mcgaugh, J.L. & Cahill, L. **2236**, 22983–22986 (1998).
- 210 2. Kensinger, E.A. *Emot. Rev.* **1**, 99–113 (2009).
- 211 3. Szöllősi, Á. & Racsmány, M. *Mem. Cogn.* **48**, 1032–1045 (2020).
- 212 4. Talmi, D. *Curr. Dir. Psychol. Sci.* **22**, 430–436 (2013).
- 213 5. Yonelinas, A.P. & Ritchey, M. *Trends Cogn. Sci.* **19**, 259–267 (2015).
- 214 6. Ben-Yakov, A., Eshel, N. & Dudai, Y. *J. Exp. Psychol. Gen.* **142**, 1255–1263 (2013).
- 215 7. Sols, I., DuBrow, S., Davachi, L. & Fuentemilla, L. *Curr. Biol.* **27**, 3499-3504.e4 (2017).
- 216 8. Logothetis, N.K. et al. *Nature* **491**, 547–553 (2012).
- 217 9. Skelin, I. et al. *Proc. Natl. Acad. Sci. U. S. A.* **118**, (2021).
- 218 10. Buzsáki, G. *Hippocampus* **25**, 1073–1188 (2015).
- 219 11. Wu, C.T., Haggerty, D., Kemere, C. & Ji, D. *Nat. Neurosci.* **20**, 571–580 (2017).
- 220 12. Jadhav, S.P., Kemere, C., German, P.W. & Frank, L.M. *Science (80-)* **336**, 1454–1458 (2012).
- 221 13. Leal, S.L., Tighe, S.K. & Yassa, M.A. *Neurobiol. Learn. Mem.* **111**, 41–48 (2014).
- 222 14. Zheng, J. et al. *Neuron* **102**, 887-898.e5 (2019).
- 223 15. McGaugh, J.L. *Annu. Rev. Psychol.* **66**, 1–24 (2015).
- 224 16. Bragin, A., Engel, J., Wilson, C.L., Fried, I. & Buzsáki, G. *Hippocampus* **9**, 137–142 (1999).
- 225 17. Genzel, L. et al. *Philos. Trans. R. Soc. B Biol. Sci.* **375**, 4–6 (2020).
- 226 18. Wixted, J.T. et al. *Proc. Natl. Acad. Sci. U. S. A.* **111**, 9621–9626 (2014).
- 227 19. Lopes-dos-Santos, V. et al. *Neuron* **100**, 940-952.e7 (2018).
- 228 20. Girardeau, G., Inema, I. & Buzsáki, G. *Nat. Neurosci.* **20**, 1634–1642 (2017).
- 229 21. Trouche, S., Pompili, M.N. & Girardeau, G. *Curr. Opin. Physiol.* **15**, 230–237 (2020).
- 230 22. Joo, H.R. & Frank, L.M. *Nat. Rev. Neurosci.* **19**, 744–757 (2018).
- 231 23. McGaugh, J.L. *Proc. Natl. Acad. Sci. U. S. A.* **110**, 10402–10407 (2013).



237

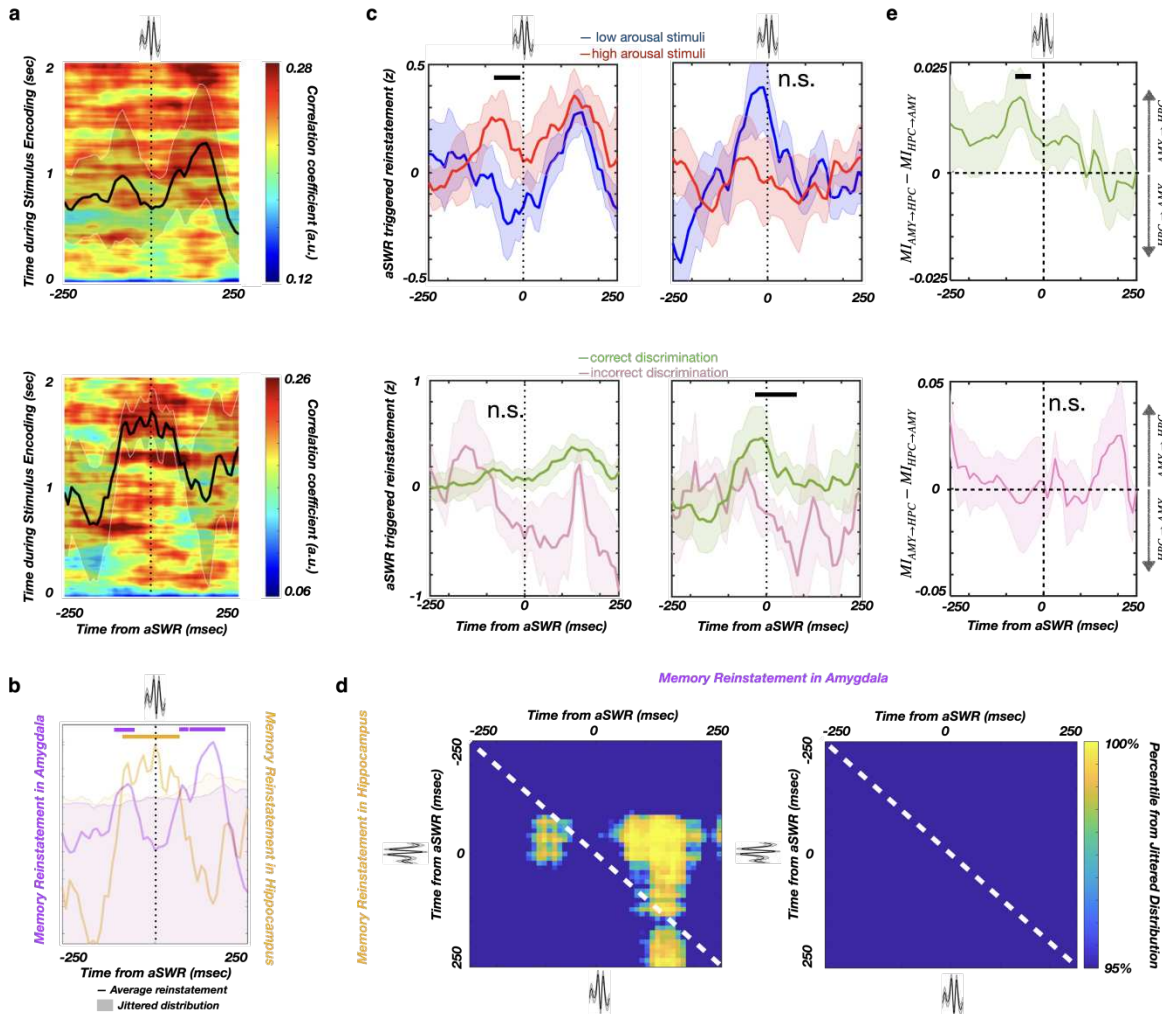
238 **Fig. 1. Memory discrimination is more accurate for emotional stimuli.**

239 **a**, Task structure: subjects are presented with an image (Stimulus encoding). Following  
 240 presentation, they rate the valence of the image as negative, neutral, or positive (Post-  
 241 Encoding/Response). Once all images are presented and rated, subjects are presented  
 242 with 3 types of stimuli - Repeat (identical), Lure (slightly different) or Novel (stimuli not  
 243 seen during encoding) - and classify each stimulus as “old” or “new.” **b**, Correct  
 244 discrimination is highest for Novel stimuli ( $93.9 \pm 1.4\%$ ; median  $\pm$  SEM), followed by  
 245 Repeats ( $89.4 \pm 2.4\%$ ) and Lures ( $61.5 \pm 3.7\%$ ). Paired t-test: Novel vs. Repeat,  $*p =$   
 246  $0.016$ ,  $t = 3.33$ ,  $df = 6$ ; Novel vs. Lure,  $***p < 0.001$ ,  $t = 8.36$ ,  $df = 6$ ; Repeat vs. Lure,  $***p <$   
 247  $0.001$ ,  $t = 6.13$ ,  $df = 6$ . **c**, Correct discrimination of Lure stimuli is positively associated  
 248 with encoded stimulus-induced arousal ( $*p = 0.047$ ,  $\beta = 0.3 \pm 0.12$ ,  $t = 1.98$ ,  $df = 452$ ,  
 249 logistic linear mixed-effect model) and valence ( $p = 0.137$ ,  $\beta = 0.15 \pm 0.09$ ,  $t = 1.48$ ,  $df =$   
 250  $452$ ), while negatively associated with similarity ( $*p = 0.039$ ,  $\beta = -0.24 \pm 0.00$ ,  $t = -2.06$ ,  $df =$   
 251  $452$ ). The  $\beta$  sign and magnitude indicate effect direction and strength, respectively.  
 252 Dots correspond to individual subjects. **d**, Probability of Lure correct discrimination as a  
 253 function of SI and stimulus-induced arousal. The solid line shows the actual proportion  
 254 of ‘New’ responses (y-axis) as a function of Lure stimulus SI (x-axis) for low arousal (blue)  
 255 or high arousal stimuli (red). The low/high arousal groups were created using the median  
 256 split.



257

258 **Fig. 2. The post-encoding aSWR occurrence predicts the stimulus-induced arousal**  
259 **and memory discrimination.** **a**, Reconstructed locations of hippocampal (blue) and  
260 amygdala electrodes (red). **b**, The aSWR grand average waveform ( $n = 4689$  aSWRs in 6  
261 hippocampal channels, 6 subjects). **c**, The aSWR occurrence is significantly higher  
262 following encoding of arousing (top right;  $*p = 0.03$ ) and later correctly discriminated  
263 stimuli (bottom right,  $*p = 0.03$ ). The aSWR occurrence was showing no conditional  
264 differences during stimulus encoding (left column,  $p$ 's  $> 0.05$ ).



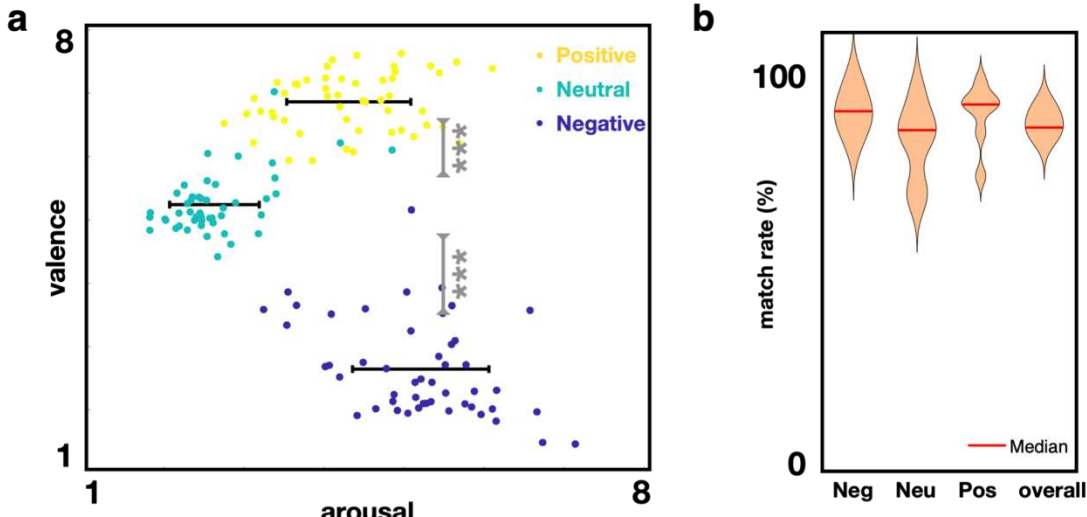
265

**Fig. 3. Memory reinstatement in the hippocampus and amygdala around aSWR. a,**  
 266 aSWR-locked reinstatement in the amygdala (top) and hippocampus (bottom) during the  
 267 post-encoding period (line and shaded areas represent the mean  $\pm$  SEM). **b,**  
 268 Reinforcement is greatest around the time of aSWRs as shown by comparison with the  
 269 null-distribution (within  $\pm$  250 msec). Shaded areas denote the null-distribution 95%  
 270 confidence interval. Reinforcement in the hippocampus overlaps with aSWR peak  
 271 (orange), while reinforcement in the amygdala peaks prior to and after the aSWR  
 272 (magenta). **c,** aSWR-locked reinstatement in the amygdala is stronger for arousing stimuli  
 273 (top left,  $p = 0.035$ , see Methods) but is not associated with subsequent discrimination  
 274 (bottom left,  $p = 0.066$ ). Reinforcement in the hippocampus is robust for correctly  
 275 discriminated stimuli (bottom right,  $p = 0.008$ , see Methods) but does not depend on  
 276 stimulus-induced arousal (top right,  $p > 0.1$ ). **d,** The aSWR-locked joint reinstatement in  
 277 the hippocampus and amygdala for the correct (left) and incorrect (right) discrimination  
 278

279 trials. Reinstatement in the amygdala starts 100 msec prior to the aSWR peak, followed  
280 by reinstatement in the hippocampus (-50 to 200 msec). There is no significant joint  
281 reinstatement during incorrect discrimination trials, suggesting that the cross-structure  
282 joint reinstatement may be required for correct discrimination. **e**, Mutual information (MI)  
283 difference for the amygdala (AMY) and hippocampal (HPC) memory reinstatement time-  
284 courses, during the post-encoding aSWR windows (correct discrimination - top, incorrect  
285 discrimination - bottom). Positive values denote stronger AMY→HPC directionality. A  
286 temporal cluster of significant MI difference (AMY→HPC) is present before aSWR peak  
287 time(-70 to -30 msec) after encoding of correctly discriminated stimuli (top;  $p = 0.038$ , see  
288 Methods), indicating that hippocampal reinstatement is better predictable by amygdala  
289 reinstatement than vice versa. This effect is present only during the post-encoding period  
290 for correctly discriminated stimuli (top), but not for the incorrectly discriminated stimuli

291 **Extended data**

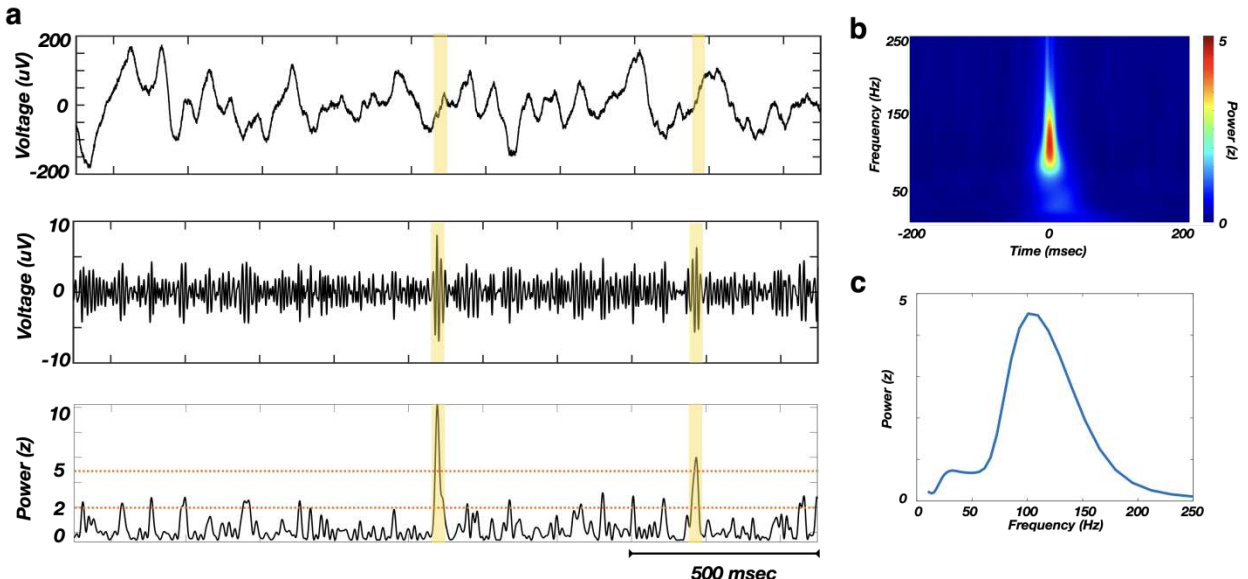
292



293

294

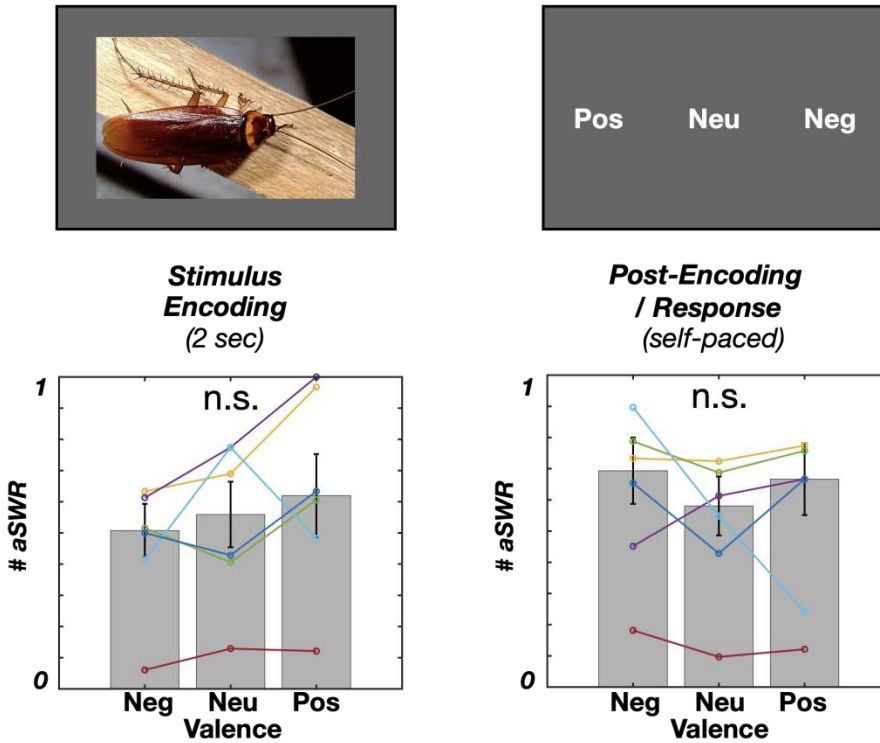
295 **Extended Data Fig. 1. a**, Positive and negative valenced stimuli are associated with  
296 higher stimulus-induced arousal, relative to neutral valence stimuli (\*\*p<0.001, Wilcoxon  
297 rank-sum test). **b**, Stimuli valence ratings of study subjects are highly similar to the  
298 healthy population (match rate =  $85.3 \pm 1.3\%$ ).



299

300 **Extended Data Fig. 2. Awake SWR detection.** **a**, Examples of several detected aSWRs  
301 (yellow highlights), showing the raw trace (top), filtered trace (80 - 150 Hz range, middle)  
302 and z-scored envelope of filtered trace (bottom). Detection is based on double-threshold  
303 (orange dashed lines) crossing of z-scored power (80-150 Hz) for the period of 20-100  
304 msec. **b**, Z-scored power spectral density of average detected aSWR. **c**, Z-scored power  
305 during aSWR windows shows a bump in the 80-150 Hz range. This suggests that the  
306 aSWRs are not detected during signal artifact periods, which would reflect as a  
307 broadband power increase. In addition, detected aSWRs are not detected during non-  
308 specific increase in broadband gamma power or pathological high-frequency oscillations  
309 (> 200 Hz).

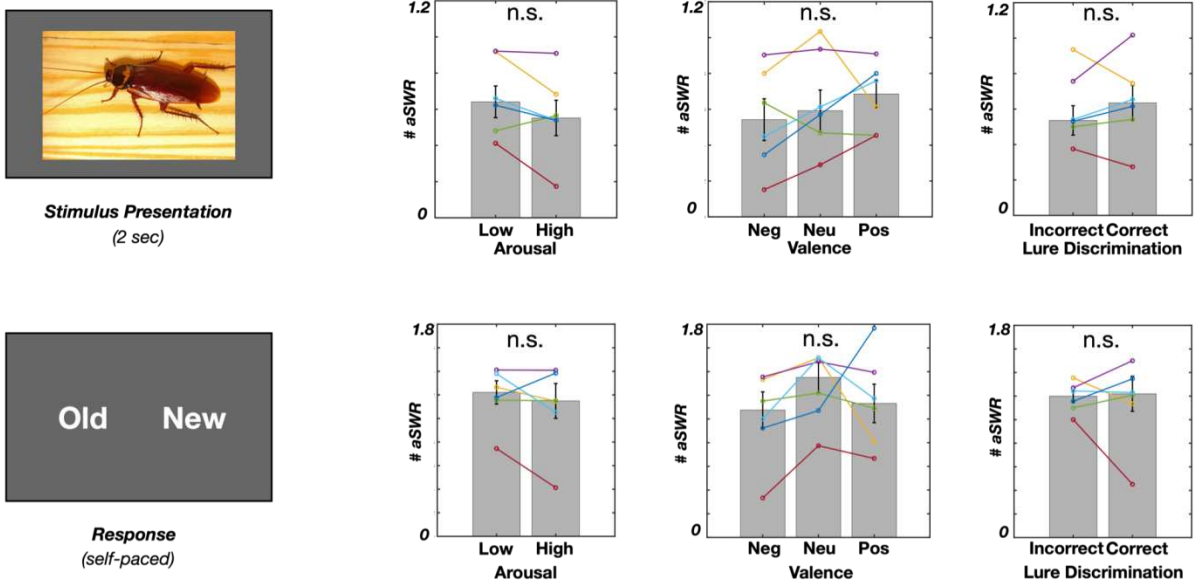
a



310

311 **Extended Data Fig. 3. Stimulus valence is not significantly associated with aSWR**  
312 **occurrence during encoding stage. a, Stimulus encoding phase:  $F(2, 15) = 0.67, p =$**   
313  **$0.53$ ; Post-encoding:  $F(2, 15) = 0.25, p = 0.77$ , One-way ANOVA). The data from**  
314 **individual subjects are color-coded.**

a

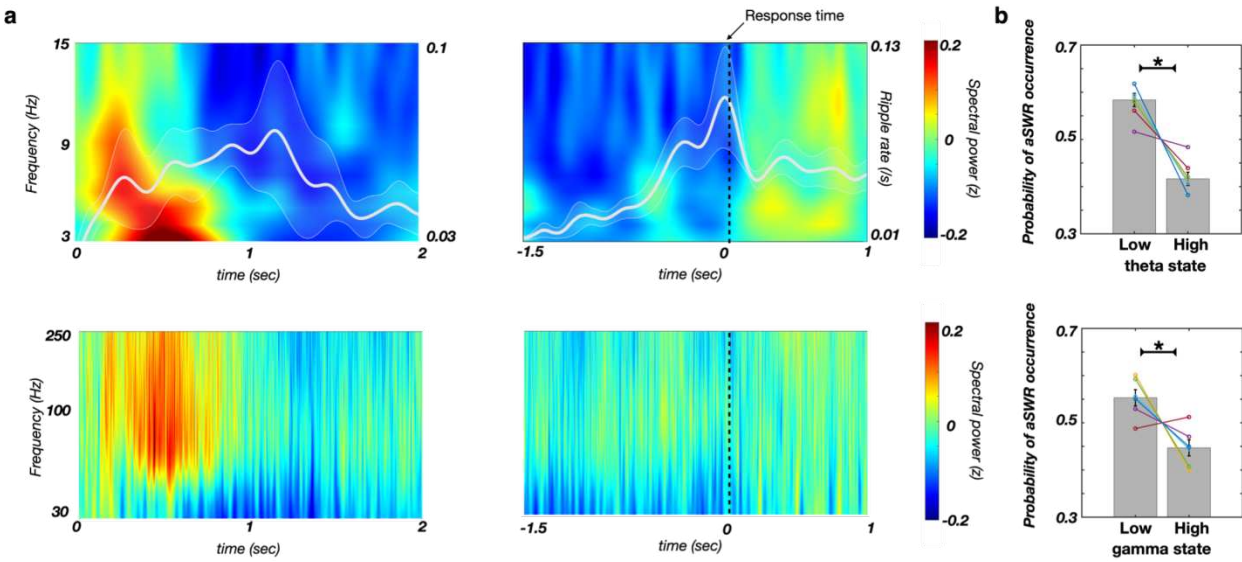


315

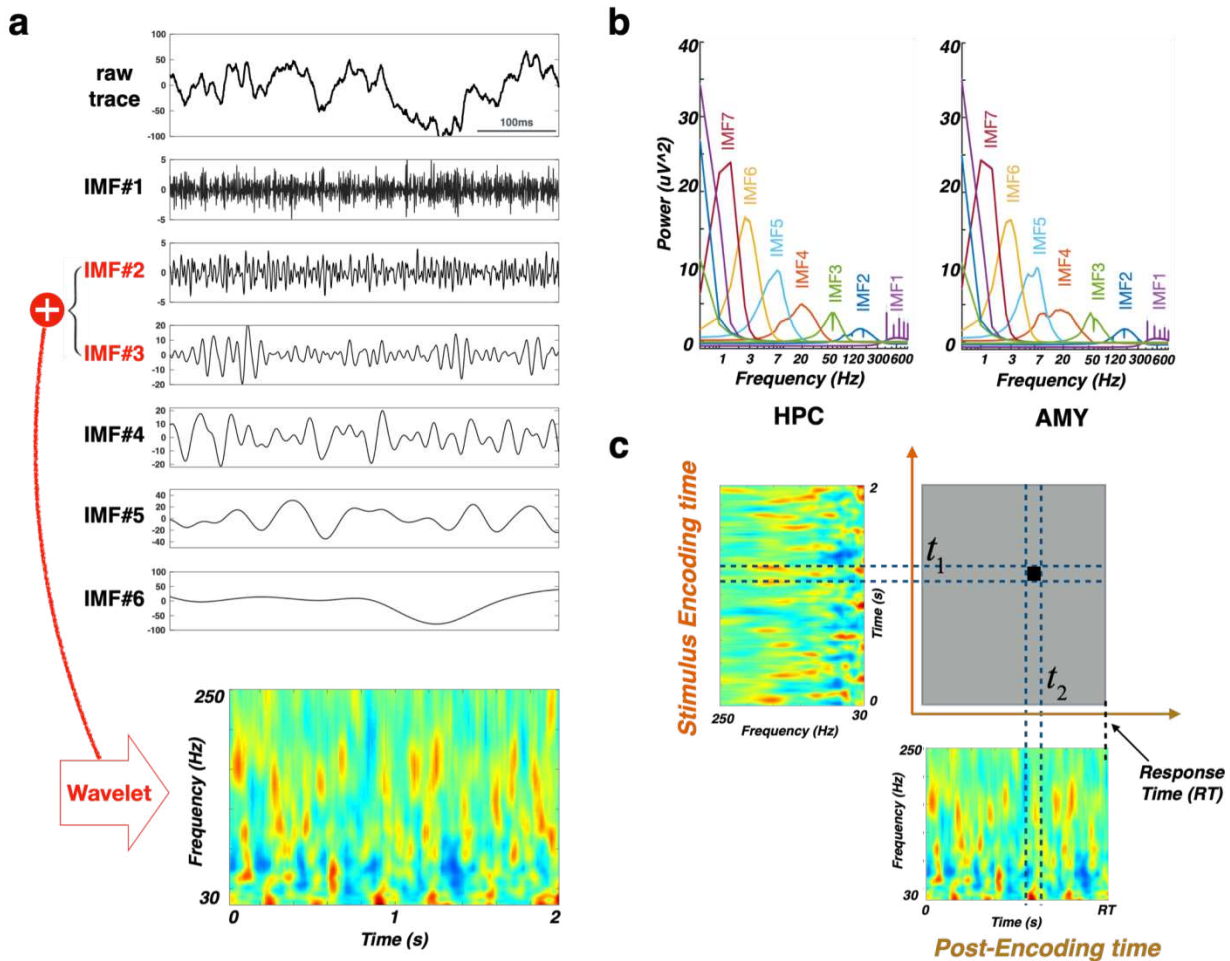
316 **Extended Data Fig. 4. The aSWR occurrence during retrieval task stage is not**  
317 **associated with stimulus-induced arousal, valence or correct discrimination.**

318 **Arousal:** Stimulus presentation (top row),  $p = 0.11$ ,  $z = 1.57$ ; Response (bottom row),  $p =$   
319  $0.17$ ,  $z = 1.36$ , Wilcoxon signed-rank test. **Valence:** Stimulus presentation,  $p = 0.69$ ,  $F(2,$   
320  $15) = 0.69$ ; Response,  $p = 0.51$ ,  $F(2, 15) = 0.71$ , One-way ANOVA). **Correct**  
321 **discrimination:** Stimulus presentation:  $p = 0.6$ ,  $z = -0.52$ ; Response:  $p = 0.92$ ,  $z = 0.11$ ,  
322 Wilcoxon signed-rank test).

323



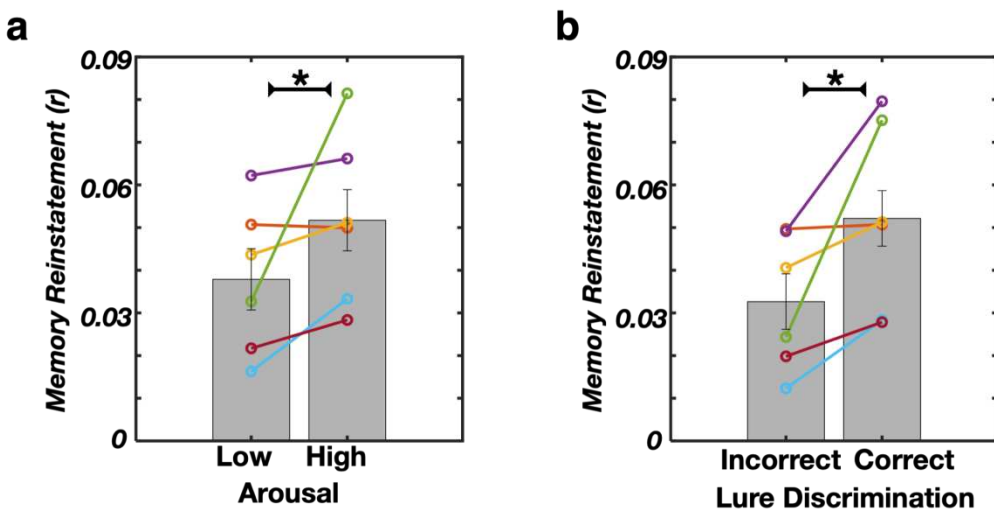
324 **Extended Data Fig. 5. aSWRs occur predominately outside of high theta or**  
325 **broadband gamma periods. a,** Low frequency (top, color) and high frequency  
326 spectrogram (bottom, color), and aSWR rate (white line) during the stimulus encoding  
327 (left) and post-encoding (right, response-locked) periods. **b,** The probability of aSWR  
328 occurrence is lower during the high theta state (top,  $p = 0.017$ ,  $z = 2.1$ , one-tailed  
329 Wilcoxon signed-rank test), or during high gamma state (bottom,  $p = 0.028$ ,  $z = 1.9$ , one-  
330 tailed Wilcoxon signed-rank test). Theta/gamma state classification was based on the  
331 power median split (for details, see 'Dual state analysis').



332

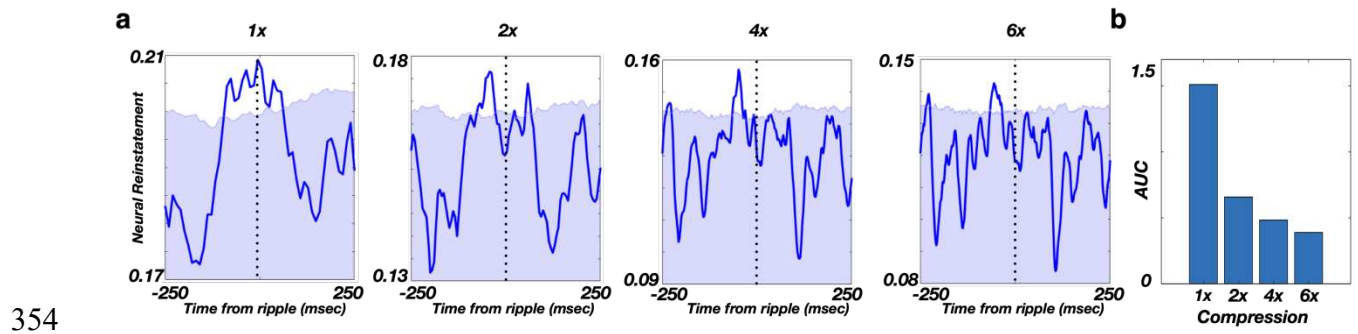
333 **Extended Data Fig. 6. Overview of Ensemble Empirical Mode Decomposition**  
 334 **(EEMD) and representational similarity analysis (RSA) methods.** **a**, An example  
 335 hippocampal raw iEEG trace (top) was decomposed into multiple intrinsic mode functions  
 336 (IMFs; lower 6 panels). IMFs within the HFA range ( $\text{IMF}_2$  and  $\text{IMF}_3$ ) were used for HFA  
 337 reconstruction. The HFA time-frequency matrix (bottom) was estimated using wavelet  
 338 transformation (for details, see Time-frequency representation of the HFA). **b**, Power  
 339 spectral density (mean  $\pm$  SEM) of the IMFs decomposed from the hippocampal (left) and  
 340 amygdala (right) electrodes. IMF spectral features were consistent across subjects and  
 341 structures, with mean center frequencies in delta ( $\text{IMF}_7$ ), theta ( $\text{IMF}_6$ ,  $\text{IMF}_5$ ), alpha/beta  
 342 ( $\text{IMF}_4$ ), gamma ( $\text{IMF}_3$ ), high-gamma bands ( $\text{IMF}_2$ ), and the noise term ( $\text{IMF}_1$ ). The HFA  
 343 time series were estimated by summing the IMFs with center frequencies  $> 30$  Hz ( $\text{IMF}_2$   
 344 and  $\text{IMF}_3$ ). **c**, The similarity matrix (top right) was constructed by computing the power  
 345 spectrum vector (PSV) Spearman's correlations for each combination of stimulus  
 346 encoding (top left) and post-encoding (bottom right) time bins.

347



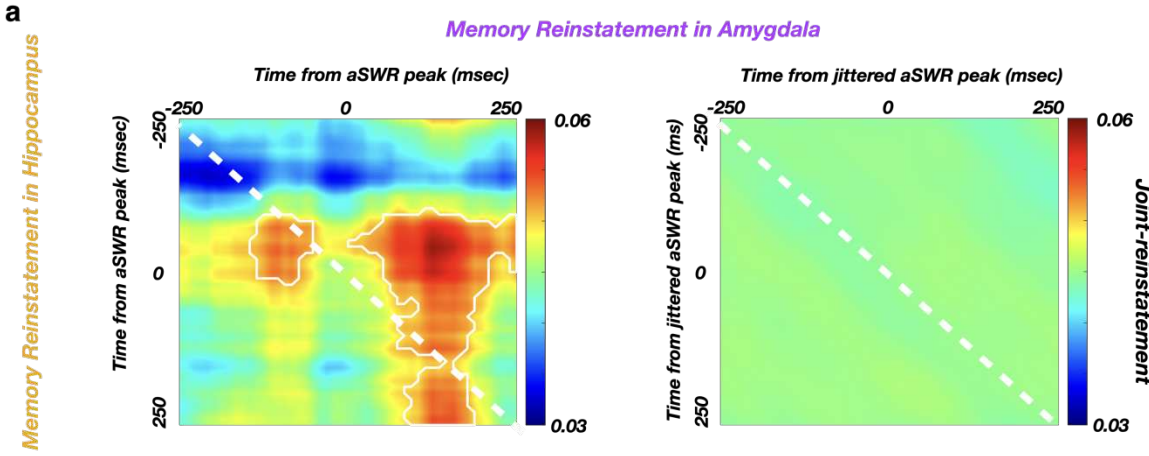
348

349 **Extended Data Fig. 7. Post-encoding aSWR-locked reinstatement (amygdala and**  
350 **hippocampus combined) is increased for high stimulus-induced arousal and**  
351 **correctly discriminated stimuli. a, Arousal:  $*p = 0.046, z = -1.991$ , Wilcoxon signed-**  
352 **rank test. b, Correct discrimination:  $*p = 0.028, z = -2.201$ , Wilcoxon signed-rank test).**  
353 Data from individual subjects is color-coded.



355 **Extended Data Fig. 8. Post-encoding aSWR-locked memory reinstatement in the**  
356 **hippocampus is strongest without time compression.** a, aSWR-locked hippocampal  
357 reinstatement during the post-encoding response period, across different temporal  
358 compression factors. Memory reinstatement strength area under curve (AUC) is defined  
359 as enclosed by the reinstatement trace (blue line) and 95% percentile of empirical null-  
360 distribution (blue shading upper limit). AUC reflects the memory reinstatement strength at  
361 different compression factors. b, Memory reinstatement strength is highest with no  
362 compression.

363



364 **Extended Data Fig. 9. Joint cross-structure memory reinstatement occurs**  
365 **selectively during aSWR time windows. a,** Average joint cross-structure reinstatement  
366 (hippocampus and amygdala) relative to aSWR peak times (left) and relative to jittered  
367 aSWR peak times (right). The white line encircles the periods of significant joint cross-  
368 structure memory reinstatement (Fig. 3d). The color scale represents the Spearman  
369 correlation between the encoding stimulus presentation and post-encoding aSWR  
370 windows. The absence of significant joint cross-structure memory reinstatement following  
371 the jittering of aSWR peak times (right) reveals the specificity of cross-structure  
372 reinstatement to aSWR windows.

Subject	Gender	Age
<b>S1</b>	<b>M</b>	<b>21</b>
<b>S2</b>	<b>F</b>	<b>58</b>
<b>S3</b>	<b>M</b>	<b>24</b>
<b>S4</b>	<b>F</b>	<b>55</b>
<b>S5</b>	<b>M</b>	<b>23</b>
<b>S6</b>	<b>M</b>	<b>29</b>
<b>S7</b>	<b>F</b>	<b>21</b>

373

374 Extended Data Table 1. Demographic information for the study subjects.

	<b>Hippocampus</b>	<b>Amygdala</b>
<b>IMF#1</b>	420 Hz	420 Hz
<b>IMF#2</b>	159 Hz	184 Hz
<b>IMF#3</b>	57.5 Hz	53 Hz
<b>IMF#4</b>	20 Hz	18 Hz
<b>IMF#5</b>	8 Hz	7.5 Hz
<b>IMF#6</b>	2.5 Hz	3 Hz
<b>IMF#7</b>	1.5 Hz	1 Hz
<b>IMF#8</b>	0.5 Hz	0.5 Hz
<b>IMF#9</b>	< 0.5 Hz	< 0.5 Hz
<b>IMF#10</b>	< 0.5 Hz	< 0.5 Hz

375

376    Extended Data Table 2. Center frequencies of the IMFs in the hippocampus and  
377    amygdala.

378 **Methods**

379 **Subjects**

380         Intracranial electroencephalography (iEEG) recordings were obtained from 7  
381 subjects (3 females; mean age  $\pm$  SD = 33  $\pm$  16), undergoing presurgical monitoring of  
382 epileptic foci at the University of California Irvine Medical Center (UCIMC) Epilepsy  
383 Monitoring Unit. The individual subject demographic information is shown in Table 1. Only  
384 the subjects with the correct discrimination rate of Novel trials  $\geq$  85% (see Emotional  
385 memory encoding and discrimination task) were included in the analysis. Electrode  
386 placements were determined entirely based on clinical considerations. All the research  
387 procedures were approved by the UCI Institutional Review Board and data was collected  
388 following informed consent.

389

390 **Statistics**

391         All the statistical tests were performed with the individual subject as the unit of  
392 analysis. Unless stated otherwise, all the parametric statistical tests (e.g., Wilcoxon  
393 signed-rank test, t-test) were two-tailed. The effects of valence, stimulus-induced arousal  
394 and similarity on stimulus discrimination (Fig. 1c) were assessed using the logistic linear  
395 mixed-effect model (for details, see Behavioral Analysis). Conditional comparisons of  
396 aSWR occurrence (correct/incorrect discrimination or high/low arousal; Fig. 2c) were  
397 done using the Wilcoxon signed rank test ( $p < 0.05$ ). Statistical significance of aSWR-  
398 locked memory reinstatement strength (Fig. 3b) was assessed by comparing the real test  
399 statistics with empirical null distribution, obtained using Monte Carlo method (for details,  
400 see Representational Similarity Analysis). We implemented the cluster-based  
401 nonparametric permutation test<sup>1</sup> to assess the conditional differences (correct/incorrect  
402 discrimination or high/low arousal) of memory reinstatement strength (Fig. 3c), mutual  
403 information (Fig. 3e), by randomly shuffling the conditional trial labels 1000 times (for  
404 details, see Representational Similarity Analysis). Similarly, the significant temporal  
405 windows for the cross structure aSWR-locked joint memory reinstatement (Fig. 3d) were  
406 assessed by comparing to empirical null distribution (for details, see Joint-reinstatement  
407 Analysis).

408

409 **Emotional memory encoding and discrimination task**

410         The emotional memory encoding and discrimination (EMOP) task consists of  
411 encoding and discrimination blocks. During the encoding block (148 trials), each trial

412 consists of a cross fixation (1000 msec), followed by stimulus encoding (2000 msec) and  
413 self-paced post-encoding response period (up to 2000 msec). During the post-encoding  
414 response period, subjects are asked to classify the stimulus emotional valence as either  
415 negative, neutral or positive, using the corresponding laptop key. During the retrieval  
416 block (290 trials), trial time structure is identical to encoding phase. Following the cross  
417 fixation (1000 msec), the subjects are presented for 2000 msec with a stimulus identical  
418 (Repeat, 54 trials), slightly different (Lure, 97 trials) or unrelated (Novel, 139 trials) to  
419 previously encoded stimuli. Next, during the self-paced memory discrimination epoch (up  
420 to 2000 msec), subjects are asked to discriminate if the presented stimulus was seen  
421 during encoding (Old) or not (New). Correct discrimination is defined as classifying the  
422 Repeat stimuli as Old and Lure or Novel stimuli as New. The stimuli were selected from  
423 the continuous distributions across the valence and stimulus-induced arousal axes  
424 (Extended Data Fig. 1). The same set of stimuli was used across subjects. In addition,  
425 the valence, arousal and similarity of each stimulus were rated by separate cohorts of  
426 healthy subjects. Specifically, a first cohort ( $N = 50$ , 32 females; age mean  $\pm$  SD =  $22 \pm 5$ )  
427 rated the stimulus emotional valence on a continuous scale (range 1-9, with 1 denoting  
428 the most negative, 9 the most positive, and 5 neutral valence). Stimuli were assigned in  
429 Negative (valence  $\leq 3.5$ ), Neutral ( $3.5 > \text{valence} < 6$ ) or Positive (valence  $\geq 6$ ) groups.  
430 Another cohort of healthy subjects ( $N = 16$ , 4 females; age mean  $\pm$  SD =  $23 \pm 5$ ) rated the  
431 stimulus-induced emotional arousal on a scale 1 - 9 (1 being the least and 9 being the  
432 most arousing). Finally, a third cohort ( $N = 17$ , 11 females; age mean  $\pm$  SD =  $20 \pm 1$ )  
433 examined relative similarity on the scale 1-8<sup>2</sup>. The high correspondence of stimulus  
434 valence ratings obtained from study subjects and healthy population (match rate =  $85.3 \pm$   
435 1.3%) suggests the intact emotional processing in study subjects (Extended Data Fig. 1).  
436

### 437 **Behavioral Analyses**

438 To assess the effects of valence, stimulus-induced arousal and similarity on Lure  
439 stimulus discrimination, we implemented the logistic linear mixed-effect model

$$440 \quad y = \beta X + u Z + \varepsilon.$$

441 In this model,  $y$  indicates the responses across the individual Lure discrimination trials (0-  
442 Old; 1-New),  $X = [x_1, x_2, x_3]^T$  denotes three fixed effect regressors (encoded stimulus  
443 valence and arousal as well as similarity between the encoded and Lure stimulus),  $Z =$   
444  $[z_1]^T$  denotes random effect regressor (subject identity),  $\beta$  and  $u$  denote the fixed and  
445 random-effect regression coefficients, and  $\varepsilon$  denotes the error term. The model includes

446 random intercept to incorporate individual subject differences. We normalized the  
447 valence, stimulus-induced arousal and similarity values relative to the scale of 0 to 1. The  
448 statistics reported in Fig. 1c corresponds to the fixed-effect coefficients  $\beta$ .

449

#### 450 **Data collection**

451 The behavioral experiment was administered using the PsychoPy2 software<sup>3</sup> (Version  
452 1.82.01). The laptop was placed at a comfortable distance in front of the subject. The  
453 iEEG signal was recorded using a Nihon Kohen system (256 channel amplifier, model  
454 JE120A), with an analog high-pass filter (0.01 Hz cutoff frequency) and sampling  
455 frequency 5000 Hz.

456

#### 457 **Electrode localization**

458 We localized each electrode using pre-implantation structural T1-weighted MRI  
459 scans (pre-MRI) and post-implantation MRI scans (post-MRI) or CT scans (post-CT).  
460 Specifically, we co-registered pre-MRI and post-MRI (or post-CT) scans by means of a  
461 rigid body transformation parametrized with three translation in x,y,z directions as well as  
462 three rotations using Advanced Normalization Tools (ANTs  
463 <https://stnava.github.io/ANTs/>). We implemented a high-resolution anatomical template  
464 with the label of medial temporal lobe subfields<sup>2</sup> to guide the localization for individual  
465 electrodes. We resampled the template with 1mm isotropic, and aligned it to pre-MRI by  
466 ANTs Symmetric Normalization<sup>4</sup> to produce a subject-specific template. The electrode  
467 localization was identified by comparing the subject-specific template subfield area with  
468 electrode artifacts.(Fig. 2a) The localization results were further reviewed by the  
469 neurologist (J.J.L.).

470

#### 471 **Preprocessing**

472 The signal preprocessing was done using the custom-written MATLAB code (Version  
473 9.7) and Fieldtrip Toolbox<sup>5</sup>. The 60 Hz line noise and its harmonics were removed using a  
474 finite impulse response (FIR) notch filter (ft\_preprocessing.m function in FieldTrip). The  
475 EEG signal was down-sampled to 2000 Hz, demeaned and high-passed filtered (cutoff  
476 frequency 0.3 Hz). The power spectrum density (PSD) was computed using the  
477 multitaper method with the Hanning window (ft\_freqanalysis.m function in FieldTrip). All  
478 the channels were re-referenced to the nearest white matter channel from the same  
479 depth electrode, based on the electrode localization results. The interictal epileptic

480 discharges were manually marked by an epileptologist (J.J.L.), using the  
481 `ft_databrowser.m` function in FieldTrip. The channels with severe contamination and trials  
482 containing epileptiform discharges were excluded from further analyses.

483

#### 484 **Awake sharp-wave/ripple detection**

485 Following the removal of channels with excessive epileptic activity and individual  
486 trials containing visually identified interictal epileptic discharges, awake sharp-  
487 wave/ripples (aSWRs) were detected on the remaining hippocampal channels, using the  
488 Freely Moving Animal Toolbox (FMA; <http://fmatoolbox.sourceforge.net/>). First, the iEEG  
489 traces from the trials used in the analysis were concatenated. Next, concatenated traces  
490 were bandpass-filtered (80 - 150 Hz, Chebyshev 4th order filter, function `filtfilt.m` in  
491 Matlab) and the voltage values during periods  $\pm$  75 msec around the trial onsets/offsets  
492 were set to zero, to avoid the edge effects resulting from filtering discontinuous traces.  
493 The analytical amplitude was obtained by computing the absolute value of Hilbert-  
494 transformed filtered trace (function `hilbert.m` in Matlab) and z-scored (Extended Data Fig.  
495 2a). Detected events were considered aSWRs if the z-scored analytical amplitude  
496 remained above the lower threshold ( $z = 2$ ) for 20 - 100 msec and if the peak value during  
497 this period exceeded higher threshold ( $z = 5$ ). Only the channels with  $>150$  detected  
498 aSWR events were used in the analysis. If the multiple channels from a single subject  
499 passed this criteria, a channel with highest number of detected aSWRs was selected for  
500 further aSWR-related analysis. Due to the low number of detected aSWRs, one subject  
501 was eliminated from the aSWR-related analysis.

502

#### 503 **Unsupervised decomposition of iEEG signal**

504 To assess the memory reinstatement, high-frequency activity (HFA; 30-280 Hz)  
505 was used as an indirect measure of local populational activity<sup>6-9</sup>. To avoid the effect of  
506 low-frequency harmonics on the HFA estimate, we applied the Ensemble Empirical Mode  
507 Decomposition<sup>7,10</sup> (EEMD; <https://github.com/leeneil/eemd-matlab.git>). Briefly, the EEMD  
508 decomposes a non-stationary signal into its elementary components, referred to as  
509 intrinsic mode functions<sup>10</sup> (IMFs; Extended Data Fig. 6). The procedure iteratively applies  
510 an empirical mode decomposition algorithm, while adding white noise to prevent the  
511 mode mixing<sup>10,11</sup>. Using this approach, decomposition output entirely depends on the  
512 signal's intrinsic properties, avoiding prior assumptions<sup>7,10,11</sup>. The resulting IMFs captured  
513 several canonical spectral features consistently across subjects and anatomical

514 structures (Extended Data Table 2). Finally, the HFA time-series on individual channels  
515 were reconstructed by summing the channel-specific IMFs with center frequencies > 30  
516 Hz<sup>7</sup>.

517

### 518 **Time-frequency representation of the HFA**

519 The instantaneous spectral power at each time-frequency bin was derived from the  
520 reconstructed HFA time series ( $x$ ), using a wavelet transform<sup>12,13</sup>. This approach consists  
521 of convolving the time series  $x$  with a set of Morlet wavelets, parametrized by a range of  
522 cycle numbers ( $n = 2, 3, \dots, 10$ ) at a given frequency  $f$ ,

523

524 
$$P_{f,n}(t) = |\psi_{f,n} * x(t)|, n = 2, 3, \dots, 10$$

525

526 with  $\psi_{f,n}$  defined as

527

528 
$$\psi_{f,n} = \frac{1}{B_n \sqrt{2\pi}} e^{-\frac{t^2}{2B_n^2}} e^{j2\pi f t}, \text{ where } B_n = \frac{n}{5f}$$

529

530 and computing the geometric average ( $\hat{P}(f, t)$ ) of resulting spectral power at each time-  
531 frequency bin:

532

533 
$$\hat{P}(f, t) = \sqrt[9]{\prod_{n=2}^{10} P_{f,n}(t)}.$$

534

535 This approach results in a high temporal and frequency resolution, facilitating the  
536 detection of narrow-band, transient oscillatory events<sup>12,13</sup>. The wavelet center frequencies  
537 were within 30 - 280 Hz range, with 1 Hz increments. The wavelet cycle number range (2-  
538 10) is commonly used<sup>14</sup>. To avoid the edge effects, this procedure was applied on the  
539 entire individual recording sessions, and the resulting time-frequency response matrices  
540 were segmented into trial epochs (starting -1000 msec prior to stimulus onset and ending  
541 1000 msec after the response time). The power within each trial epoch was then  
542 normalized by z-transforming each frequency bin and subtracting the average pre-trial  
543 baseline (-1000 - 0 msec, relative to stimulus onset<sup>14</sup>).

544

### 545 **Representational Similarity Analysis (RSA)**

546 The representational similarity was quantified as the Spearman correlation between  
547 the HFA power spectral vectors (PSVs), for each combination of the encoding-response

548 time bins from the same trial<sup>15–18</sup> (Extended Data Fig. 6). Specifically, the instantaneous  
549 spectral power at each frequency was estimated for 100 msec time bins (10 msec step  
550 size, 90% overlap), producing the time bin - specific power spectrum vectors (PSV),  
551 spanning the encoding (2 sec time window after stimulus onset) and post-encoding  
552 response (time window after stimulus offset and before button press) periods:

553

554 
$$\overrightarrow{PSV}_{encoding}(t_1) = [z_1(t_1), \dots, z_{n_f}(t_1)]_{encoding}$$

555

556 
$$\overrightarrow{PSV}_{response}(t_2) = [z_1(t_2), \dots, z_{n_f}(t_2)]_{response}$$

557

558 Similar to previous studies<sup>15–20</sup>, we computed Spearman’s correlation as a measure of  
559 PSV similarity between the encoding time  $t_1$  and response time  $t_2$  for each encoded  
560 stimulus,

561

562 
$$r(t_1, t_2) = \frac{Cov(rg_{\overrightarrow{PSV}_{encoding}(t_1)}, rg_{\overrightarrow{PSV}_{response}(t_2)})}{\sigma_{rg_{\overrightarrow{PSV}_{encoding}(t_1)}} \sigma_{rg_{\overrightarrow{PSV}_{response}(t_2)}}} \quad , t_1 \in [0, 2], t_2 \in [0, RT] \text{ sec}$$

563

564 , with  $rg$  representing the ranking operator on the vector  $\overrightarrow{PSV}$ , and  $\sigma$  the variance of the  
565 vector. This produced a trial-specific two-dimensional similarity matrices, containing all  
566 the combinations of encoding ( $t_1$ ) and response ( $t_2$ ) time bins (Extended Data Figure 6d).  
567 The correlation coefficients  $r$  were then Fisher transformed, with the resulting  
568 coefficients following Gaussian distribution. The region-specific (amygdala and  
569 hippocampus) similarity matrices were averaged across trials within individual subjects,  
570 and used for group-level statistical analysis.

571

## 572 **aSWR-locked memory reinstatement**

573 Memory reinstatement during individual post-encoding time bins was computed by  
574 averaging the bin-specific similarity with the encoding period (200 time bins over 2 sec),  
575 resulting in a memory reinstatement time series. To obtain the aSWR-locked memory  
576 reinstatement, we averaged the memory reinstatement within  $\pm 250$  msec around the  
577 individual aSWR peak times, separately for amygdala and hippocampus (Fig. 3a). We  
578 next tested whether the memory reinstatement is locked to aSWRs (Fig. 3b), by  
579 comparing the grand-average aSWR-locked reinstatement trace with an empirical null  
580 distribution obtained from Monte Carlo simulation. Specifically, we circularly randomly

581 jittered the aSWR peak times within  $\pm 500$  msec window for 1000 times, obtaining an  
582 empirical null distribution of memory reinstatement strength.

583

584 To test whether the aSWR-locked reinstatement is associated with stimulus-induced  
585 arousal and later discrimination (Fig. 3c), we first derived the aSWR-triggered  
586 reinstatement, a metric taking the time-locked specificity relative to aSWR peak time into  
587 account. For every per-aSWR reinstatement trace around aSWR peak time, we circularly  
588 jittered the time as the procedure described above. This results in an empirical null  
589 distribution of reinstatement (i.e., correlation coefficient) for every time point around  
590 aSWR. We normalized the real reinstatement by z-scoring with mean and standard  
591 deviation of the null distribution. We referred to the resulting z-value as aSWR triggered  
592 reinstatement and it follows Gaussian distribution. We quantified the aSWR-locked  
593 reinstatement difference between the high/low arousal and between correct/incorrect  
594 discrimination at every time point by t-test, and corrected for the multiple comparisons  
595 using cluster-based nonparametric permutation test. Specifically, we performed the  
596 group-level comparisons using paired t-test and identified contiguous time bins with the p  
597  $< 0.05$ , defined as clusters. The t-values within each cluster were summed as the cluster  
598 statistics. We created an empirical null distribution by shuffling the conditional trial labels  
599 1000 times where the maximum cluster statistics was identified for each permutation. It is  
600 considered as statistically significant if the real t-sum cluster statistics exceeded the 95%  
601 percentile of the null distribution.

602

### 603 **Cross-structure joint aSWR-locked memory reinstatement**

604 The cross-structure joint aSWR-locked memory reinstatement was obtained by  
605 calculating the outer product between the structure-specific reinstatement traces  
606 (hippocampus and amygdala) during post-encoding aSWR windows. The resulting joint  
607 reinstatement matrices were averaged across the individual aSWRs for each subject,  
608 separately for later correctly or incorrectly discriminated trials. To assess the statistical  
609 significance of joint cross-structure memory reinstatement, we performed a Monte Carlo  
610 simulation to generate an empirical null distribution by circularly jittering the aSWR peak  
611 times. The reinstatement significance was defined as exceeding the 95% percentile of  
612 null distribution (Fig. 3d).

613

### 614 **Dual states analyses**

615 Recorded periods were divided into low- and high-theta (3 - 10 Hz) or gamma (30 -  
616 250 Hz) periods, based on the subject-specific power median split. The aSWR  
617 occurrences are defined as the proportions of aSWRs occurring during each period. The  
618 aSWR occurrence comparisons between the low- and high-theta or gamma periods were  
619 performed using one-tailed Wilcoxon signed-rank test ( $p < 0.05$ ; Extended Data Figure 9).  
620

621 **Mutual information**

622 Mutual information (MI)<sup>14,21</sup> is a method for quantifying the amount of information  
623 shared between the variables of interest. In electrophysiology, MI is applied to test for the  
624 presence and directionality of information flow between the multiple time-series. We  
625 applied MI to assess the directional influence between the memory reinstatement in  
626 amygdala and hippocampus during the post-encoding aSWR windows (Fig. 3e). First, the  
627 structure-specific memory reinstatement traces from the amygdala and hippocampus  
628 were obtained around each aSWR event ( $\pm 250$  msec; see aSWR-locked memory  
629 reinstatement). Next, we calculated the MI between the amygdala and hippocampal  
630 memory reinstatement traces, using the 200 msec bin size (10 msec step size), covering  
631 the  $\pm 250$  msec window around aSWR peaks. For each time bin, the reinstatement  
632 strength was binned into 10 bins (with uniform bin count), consistently across the subjects  
633 and conditions. The MI between the time series X and Y was defined as  
634

$$635 MI(X; Y) = \sum_i^n \sum_j^m p(x_i, y_j) \log_2 p(x_i, y_j) - \sum_i^n p(x_i) \log_2 p(x_i) - \sum_j^m p(y_j) \log_2 p(y_j)$$

636  
637  
638 , where  $p(x_i)$  and  $p(y_j)$  represented the marginal probability of signals X and Y,  $p(x_i, y_j)$   
639 indicated their joint probability, while m and n represented the numbers of reinstatement  
640 strength bins for time series X and Y<sup>14,21</sup>. To test the directionality of information flow, we  
641 calculated the time-lagged MI by shifting one time series relative to another across all the  
642 time bin combinations. The  $MI_{AMY \rightarrow HPC}$  and  $MI_{HPC \rightarrow AMY}$  at individual time bins were  
643 defined as the mean of all the subsequent time-lagged MI bins in the other region<sup>14,22</sup>.  
644 We defined the MI directional influence as the significant difference between the  
645  $MI_{AMY \rightarrow HPC}$  and  $MI_{HPC \rightarrow AMY}$ , assessed using Wilcoxon signed-rank test for each time  
646 bin. Correction for multiple comparisons was performed using the cluster-based  
647 nonparametric permutation test.

648

649 **References:**

- 650 1. Maris, E. & Oostenveld, R. *J. Neurosci. Methods*  
651 (2007).doi:10.1016/j.jneumeth.2007.03.024
- 652 2. Leal, S.L., Tighe, S.K. & Yassa, M.A. *Neurobiol. Learn. Mem.* **111**, 41–48 (2014).
- 653 3. Peirce, J.W. *Front. Neuroinform.* **2**, 1–8 (2009).
- 654 4. Avants, B.B. et al. *Neuroimage* **54**, 2033–2044 (2011).
- 655 5. Oostenveld, R., Fries, P., Maris, E. & Schoffelen, J.M. *Comput. Intell. Neurosci.*  
656 **2011**, (2011).
- 657 6. Ray, S. & Maunsell, J.H.R. *PLoS Biol.* **9**, (2011).
- 658 7. Lopes-dos-Santos, V. et al. *Neuron* **100**, 940–952.e7 (2018).
- 659 8. Wixted, J.T. et al. *Proc. Natl. Acad. Sci. U. S. A.* **111**, 9621–9626 (2014).
- 660 9. Canolty, R.T. & Knight, R.T. *Trends Cogn. Sci.* **14**, 506–515 (2010).
- 661 10. Wu, Z. & Huang, N.E. *Adv. Adapt. Data Anal.* **1**, 1–41 (2009).
- 662 11. Huang, N.E. et al. *Proc. R. Soc. A Math. Phys. Eng. Sci.* **454**, 903–995 (1998).
- 663 12. Moca, V. V., Bârzan, H., Nagy-Dăbâcan, A. & Mureşan, R.C. *Nat. Commun.* **12**, 1–  
664 18 (2021).
- 665 13. Bârzan, H.2220–2224 (2020).
- 666 14. Cohen, M.X. *MIT Press* (2014).
- 667 15. Yaffe, R.B. et al. *Proc. Natl. Acad. Sci. U. S. A.* **111**, 18727–18732 (2014).
- 668 16. Lohnas, L.J. et al. *Proc. Natl. Acad. Sci. U. S. A.* **115**, E7418–E7427 (2018).
- 669 17. Zhang, H., Fell, J. & Axmacher, N. *Nat. Commun.* **9**, (2018).
- 670 18. Norman, Y. et al. *Science (80-)* **365**, (2019).
- 671 19. Pacheco Estefan, D. et al. *Nat. Commun.* **10**, (2019).
- 672 20. Staresina, B.P. et al. *Elife* **5**, 1–18 (2016).
- 673 21. Quiroga, R. & Panzeri, S. *Nat. Rev. Neurosci.* **10**, 173–185 (2009).
- 674 22. Helfrich, R.F. et al. *Nat. Commun.* **10**, 1–16 (2019).